Ferromagnetic model on the Apollonian packing

Rafael S. Oliveira[1,2] and Roberto F. S. Andrade[1]

[1]*Instituto de Física, Universidade Federal da Bahia, 40210-210, Salvador, Brazil*

[2]*Centro de Formação de Professores, Universidade Federal do Recôncavo da Bahia, 45300-000, Amargosa, Brazil*

(Received 3 July 2016; revised manuscript received 12 December 2016; published 17 January 2017)

This work investigates the influence of geometrical features of the Apollonian packing (AP) on the behavior of magnetic models. The proposed model differs from previous investigations on the Apollonian network (AN), where the magnetic coupling constants depend only on the properties of the network structure defined by the packing, but not on quantitative aspects of its geometry. In opposition to the exact scale invariance observed in the AN, the circle's sizes in the AP are scaled by different factors when one goes from one generation to the next, requiring a different approach for the evaluation of the model's properties. If the nearest-neighbors coupling constants are defined by $J_{i,j} \sim 1/(r_i + r_j)^{\alpha}$, where r_i indicates the radius of the circle i containing the node i, the results for the correlation length ξ indicate that the model's behavior depend on α. In the thermodynamic limit, the uniform model ($\alpha = 0$) is characterized by $\xi \to \infty$ for all $T > 0$. Our results indicate that, on increasing α, the system changes to an uncorrelated pattern, with finite ξ at all $T > 0$, at a value $\alpha_c \simeq 0.743$. For any fixed value of α, no finite temperature singularity in the specific heat is observed, indicating that changes in the magnetic ordering occur only when α is changed. This is corroborated by the results for the magnetization and magnetic susceptibility.

DOI: 10.1103/PhysRevE.95.012123

I. INTRODUCTION

The investigation of the collective behavior resulting from the interactions among agents in complex networks is of utmost importance for understanding the behavior of natural, social, and economic systems [1–4]. Usually one compares networks based on actual data with artificial counterparts, which can be generated by stochastic or deterministic procedures: in the first case, networks are produced with the intervenience of a random process that controls the inclusion (or not) of an edge between any two nodes [5–7]. The second approach consists of constructing deterministic structures, by successively using a set of geometric rules that leads to a hierarchy of networks with a growing number of nodes and edges at successive generations [8–10].

The behavior of above quoted systems can profit from the studies on the behavior of magnetic spin models on networks, where the focus is to investigate the conditions for the emergence of phase transitions and to characterize the critical behavior. It is known that complex networks may or may not show magnetic phase transition at a well-defined critical temperature T_c [11–14]. If the network building procedure depends on one parameter X, it frequently happens that a phase transition can be found and located in a phase diagram $T_c = T_c(X)$. This is the case, for instance, of the homogeneous Ising model on the generalized Barabasi-Albert (BA) scale-free network [7]. Here, X represents the exponent γ of the node degree distribution $P(k) \sim k^{-\gamma}$. Three disjoint γ intervals $[0,3]$,$(3,5]$, and $(5,\infty)$ have been identified where, respectively, magnetic ordering occurs at all temperatures, a phase transition is observed at a finite temperature, and no magnetic ordering is observed for $T > 0$ [11–13].

The Apollonian network (AN) has been used as a prototype of a deterministically generated complex network since it shares many of the features that are found in actual or randomly generated networks [9]. The ordering properties of several magnetic models on the AN are similar to those of the BA network in the $[0,3]$ interval [15]. For a degree-dependent (k-dependent) exchange coupling given by $J_{ij} = J_{ij}(k_i,k_j; X = \mu) = J_0/(k_i k_j)^{\mu}$, the model shows magnetic ordering at all temperatures when $\mu < 1$, and no ordering at $T > 0$ when $\mu \geqslant 1$ [16]. This contrasts with the observed behavior for Ising models on scale-free networks with the dependence of the magnetic coupling on the node degree [17,18]. Hence, no interval or single value of μ where a finite critical temperature has been observed. Contrary to usual situations where the network topology is not directly related to geometry, e.g., Cayley tree or diamond hierarchical lattices, the structure of AN can be traced back to the Apollonian packing (AP), which is the solution of a well-defined geometrical problem, namely the optimal covering of a planar domain by circles.

This work explores the rare opportunity of including geometrical elements into a magnetic model defined on a complex network. Here we investigate the thermodynamical properties of a ferromagnetic Ising model on the AP. Although it shares the same topological structures with AN, this distinction is made to emphasize the fact that the coupling constants between spins placed on the center of tangent circles i and j are given by $J_{i,j} = J_{i,j}(r_i,r_j)$, where r_i is the radius of the circle i in the AP. This explicit dependence of J_{ij} on a geometrical property of each circle is the main distinction to previous models [16,19,20], where the interaction was influenced only by the network topology. This gives rise to a comparatively richer interaction pattern, as two pairs of nodes with the same degree may be at different geographic distance and will not share the same interaction constant. The ultimate goal is to investigate whether, by considering the influence of the AP geometry on the coupling constants, a magnetic model can show a finite nonzero critical temperature.

The rest of this paper is organized as follows: Section II discusses basic properties of the Apollonian geometry: AP, AN, and the proposed model. Details of the used TM scheme to evaluate the thermodynamical properties are presented in Sec. III. We discuss our main results in Sec. IV, emphasizing

the emergence of a crossover in the parameter α, which gauges the dependence of the coupling constant J_{ij} on the radii r_i and r_j. Finally, Sec. V closes the paper with our concluding remarks.

II. APOLLONIAN PACKING MAGNETIC MODEL

The two-dimensional AP represents the solution to the problem of optimally covering a finite domain of the plane with circles. Independently of the domain's shape, the asymptotic solution amounts to finding an infinite set of three mutually tangent circles. Thus, the simplest geometrical situation starts with three touching circles centered at the vertices of an equilateral triangle, as illustrated in Fig. 1 of Ref. [9]. All further circles in the packing can be recursively evaluated with the help of the Descartes circle theorem and the complex Descartes theorem [21], which provide analytical expressions for the radius and coordinates of the center of a circle that is tangent to all three previously chosen tangent circles. The AN is obtained by linking the centers of all tangent circles, reproducing a triangular structure that emerges when a circle is drawn inside the region bounded by three touching circles. Other more complex packing geometries, and corresponding networks, of tangent circles can be also obtained [22].

We remind that it is possible to obtain the same topological AN structure by a simple recurrence rule, which does not require the precise knowledge of the circles in the AP [15,22]. This procedure amounts to starting at generation $g = 1$ with an equilateral triangle in a plane. Next, a node is inserted inside the triangle and connected to all three vertices, forming three new triangles at $g = 2$. This same procedure is used to obtain the $g + 1$ generation network, namely by inserting a node inside each triangle in the generation g and connecting it to the vertices in that triangle. Another way to proceed with the network construction explores the fact that the $g + 1$ generation network can be obtained by joining three deformed units of the previous g generation network. These observations allow to obtain the total number of nodes N and edges B in the g generation according to the expressions $N(g) = (3^{g-1} + 5)/2$ and $B(g) = (3 + 3^g)/2$, so that $B(g)/N(g) \to 3$ when $g \to \infty$ [9]. When a node is inserted into the network, it generates three new triangles, so that the total number of triangles at generation g is $T(g) = (3^g - 1)/2$. If we use lower case letters to indicate the number of elements that are introduced into the network on generation g, we obtain $n(g) = N(g) - N(g-1) = (3^{g-1} - 3^{g-2})/2$ and $b(g) = t(g) = (3^g - 3^{g-1})/2$. These AN topological properties are also valid for the AP, and will help us in developing an adequate method to evaluate the thermodynamical properties of the AP model.

Probably because of such simple recurrence procedures, the geometrical properties of the AP have been overlooked in large variety of models defined on the AN that only take into account its topological properties. These include disordered magnetic systems [20,23], electronic models [24,25], quantum walks [26,27], Bose-Einstein condensation [28], as well as nonstationary processes [29–31]. The same is valid for AN related networks, as the analyses of Ising models on the regularized AN's [32,33].

As anticipated in Sec. I, here we consider geometrical elements of the AP by assuming that the interactions between pairs (i, j) of Ising spins $\sigma = \pm 1$ placed at the centers of tangent circles depend on the circles radii r_i and r_j according to the expression

$$J_{ij} = J_{ij}(r_i, r_j; X = \alpha) = \frac{J_0}{(r_i + r_j)^\alpha}, \tag{1}$$

with $J_0 > 0$. This dependence aims to account for a decrease of the coupling strength with the distance between the circle's centers, where the spins are supposed to be placed. The Ising Hamiltonian is written as

$$\mathcal{H}_g = -\sum_{(i,j)} J_{ij}\sigma_i\sigma_j - h\sum_i \sigma_i, \tag{2}$$

where J_{ij} is expressed by Eq. (1), and (i, j) indicates pairs of AP tangent circles. Note that, when $\alpha = 0$, the coupling constants become independent of the packing geometry and the model reduces to the version investigated in Ref. [9].

III. TRANSFER MATRIX APPROACH

As argued before, the AN is granted an exact self-similar topological structure by the recurrent construction rules. For several models that are independent of the AP geometrical aspects, a transfer matrix (TM) formalism based on the observed self-similarity has been developed [15,16,19,20] to proceed with the numerical evaluation of the thermodynamic and magnetic properties of the system. Inspired by the strategy of obtaining the $g + 1$ generation by joining three deformed g networks, it can be noticed that the TM elements at generation $g + 1$ can be expressed as functions of the same set of elements at previous generation g. The numerical iteration of the set of maps leads, in a straightforward way, to the partition function, free energy, and related thermodynamic properties as a function of T and h.

The iteration of these maps provides values for all quantities as a function of g. If g is large enough, the intensive quantities converge to fixed values, in a process that corresponds to taking the thermodynamic limit.

In the current model, however, the dependence of J_{ij} on r_i and r_j does not allow us to obtain the $g + 1$ system by assembling three deformed units of its version at generation g. Because identical circles at generation g will be deformed differently in the squeezing process, it becomes necessary to adapt the previously used TM approach.

To treat the AP model, it becomes necessary to choose the size of the system by assigning the value $g_{\max}$, such that only circles that appear in the packing from generations 1 to $g_{\max}$ will be represented in the network. Every such circle must be fully characterized in terms of its radii and center positions, so that all coupling constants can be evaluated with the help of Eq. (1). Since the number of distinct circles grows exponentially, the value of $g_{\max}$ that can be reached turns out to be small as compared to those used in previous models that do not depend explicitly on the AP geometric features.

To proceed with the evaluation of partition function $Z_{g_{\max}}$, the usual labeling of each node or circle in the network or

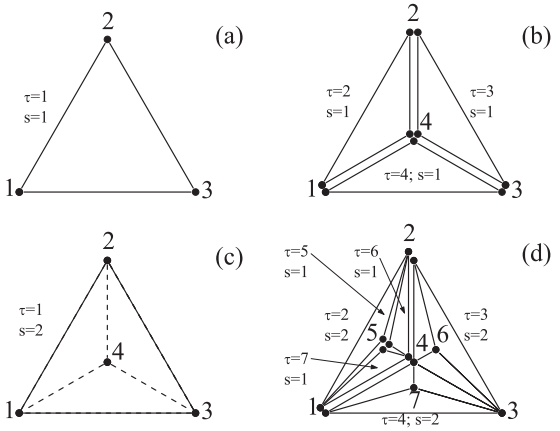

FIG. 1. (a)–(c) illustrate the first steps of the construction of the AN. The labels indicate how the TM's for each individual triangle of type $s = 1$ are combined to generate a new TM corresponding to $s = 2$ triangle. (d) indicates how to proceed to next step, when three $s = 2$ triangles are combined to form the $s = 3$ triangle.

packing is not sufficient, and it becomes necessary to identify each triangle in the network. If we start with $g = 1$, the network consists of three nodes, labeled from $i = 1$ to $i = 3$, and one triangle that receives the label $\tau = 1$. To this triangle, with no node inside it, it will be assigned a further label $s = 1$, which is called the triangle type. The next step corresponds to $g = 2$, where the system differs from the previous one by the presence of just one node $[n(g = 2) = 1]$, labeled by $i = 4$, but with three new triangles $[t(g = 2) = 3]$, labeled from $\tau = 2$ to $\tau = 4$. Each new triangle is of type $s = 1$, but the original triangle, formed by the three original nodes $i = 1,2$, and 3, now contains one node in its interior. It will be identified as a $s = 2$ triangle.

The process is illustrated in Fig. 1. The interactions in the triangle in Fig. 1(a) are described by the matrix elements defined in Eq. (4), where $i = 1, j = 2$, and $\ell = 3$, corresponding to the $\tau = 1, s = 1, g_{\max} = g = 1$ triangle. When $g_{\max} = 2$, two steps are required and Eq. (5) is used one single time. Figure 1(b) represents its right-hand side, with the nodes $i = 1, j = 2, k = 3$, and $\ell = 4$ being the vertices of the triangles $\tau_1 = 2, s = 1, g_{\max} = 2$, $\tau_2 = 3, s = 1, g_{\max} = 2$, and $\tau_3 = 4, s = 1, g_{\max} = 2$. The left-hand side of Eq. (5) is represented by Fig. 1(c), which displays the triangle $\tau_4 = 1, s = 2, g_{\max} = 2$. The dashed lines indicate that the contributions of the node $\ell = 4$ have been summed out, so that σ_4 no longer appears in the expression of the partition function. Finally, Fig. 1(d) highlights the first step for $g_{\max} = 3$, when Eq. (5) is used four times until the triangle $\tau = 1, s = 3$ is obtained. In detail, the indication how the triangle $\tau = 2, s = 2, g_{\max} = 3$, represented by the left-hand side of Eq. (5), is formed by summing over the contributions of the spin at $\ell = 5$ in a similar way as indicated in Fig. 1(b). Here, the nodes 1, 2, 4, and 5 form the following triangles: (i) $\tau = 5, s = 1, g_{\max} = 3$; (ii) $\tau = 6, s = 1, g_{\max} = 3$; (iii) $\tau = 7, s = 1, g_{\max} = 3$. For each value of τ, the corresponding nodes appear in the right-hand side of Eq. (5). After the triangles $\tau = 2, s = 2, g_{\max} = 3$ and $\tau = 3, s = 2, g_{\max} = 3$ are assembled in a similar way, the triangle $\tau = 4, s = 2, g_{\max} = 3$ is obtained by summing over the contributions of the spin states on the node 4.

The described identification of nodes and triangles will be extended for any value $1 < g \leqslant g_{\max}$: (i) $n(g)$ nodes are introduced in the network, which are labeled from $N(g-1)+1$ to $N(g)$; (ii) in the same way, $t(g)$ triangles are introduced in the network, which are labeled from $T(g-1)+1$ to $T(g)$. Each new triangle is of type $s = 1$, but triangles formed in the previous generations g' are of of type $s = g - g' + 1$. The interior of a triangle of type s contains $N(s) - 3$ nodes and $T(s) - 1$ triangles. A type s triangle inside a $g_{\max} > s$ network corresponds to a distorted version of the triangle formed by the three outmost original nodes when $s = g_{\max}$. Finally, we remark that, by construction, no triangle contains more than one vertex of the same generation $g > 1$.

Once the value of $g_{\max}$ has been selected, we start the evaluation of the $Z_{g_{\max}}$ by considering all $t(g_{\max})$ triangles in which one of the innermost sites (i.e., those included in the network when $g = g_{\max}$) is a vertex. Let us consider one such triangle, with label τ_1 and vertices labeled by i, j, and ℓ, which we indicate by (i,k,ℓ). We store the Boltzmann weights of all spin configurations involving the vertices of this triangle in the 2×4 TM $\mathcal{M}^{s,g}_{\tau_1}$:

$$\mathcal{M}^{s,g}_{\tau_1} = \begin{bmatrix} a^{s,g}_{\tau_1} & b^{s,g}_{\tau_1} & c^{s,g}_{\tau_1} & d^{s,g}_{\tau_1} \\ d^{s,g}_{\tau_1} & c^{s,g}_{\tau_1} & b^{s,g}_{\tau_1} & a^{s,g}_{\tau_1} \end{bmatrix}. \tag{3}$$

Here, the values assumed by the superscripts are $s = 1$ and $g = g_{\max}$. Because of the up-down symmetry, the matrix elements satisfy the relation $(\mathcal{M}^{s,g}_{\tau_1})_{u,v} = (\mathcal{M}^{s,g}_{\tau_1})_{3-u,5-v}$, with $u = 1,2$ and $v = 1,2,3$, and 4, as indicated in Eq. (3). They depend on the state of the three spins according to the expression

$$\langle \sigma_i | \mathcal{M}^{s,g}_{\tau_1} | \sigma_j \sigma_\ell \rangle = \exp^{[\frac{\beta}{2}(J_{ij}\sigma_i\sigma_j + J_{j\ell}\sigma_j\sigma_\ell + J_{\ell i}\sigma_\ell\sigma_i)]}, \tag{4}$$

where $\beta = 1/k_B T$. The matrix lines $u = 1,2$ correspond to $\sigma_i = +1, -1$. The column label assumes the values $v = 1,2,3,4$ according to the following states of the (σ_j,σ_ℓ) pair: $[(+1,+1),(+1,-1),(-1,+1),(-1,-1)]$. For the sake of definitiveness, let us assume that the node ℓ was introduced in the network in the generation $g_{\max}$. By construction, it forms two further triangles labeled by τ_2 and τ_3, with the pairs of nodes (i,k) and (j,k), respectively. Note also that the network construction procedure warrants that one of the nodes i, j, or k was inserted in the network at generation $g_{\max} - 1$, and that they form a $s = 2$ triangle, which we label by τ_4. For the sake of definitiveness, let us assume that the node k was inserted into the network at generation $g_{\max} - 1$.

In the same way as expressed by Eq. (3), two similar TM's $\mathcal{M}^{s,g}_{\tau_2}$ and $\mathcal{M}^{s,g}_{\tau_3}$ are constructed to account for the triangle configurations involving the spins in the vertices (j,k,ℓ) and (k,i,ℓ). Once the degree of node ℓ is 3, and it has connections to the nodes i, j, and k, we can start the evaluation of $Z_{g_{\max}}$ by performing the partial trace over all configurations involving the spin σ_ℓ. Since the result of the partial trace still depends on the eight different configurations for the spins at the nodes i, j, and k, we can store the different values in a 2×4 TM $\mathcal{M}^{s=2,g}_{\tau_4}$. Note that s now assumes a different value. Once the value of $g_{\max}$ is selected, the value of the superscript is always $g = g_{\max}$. However, for the sake of a simpler notation, we will keep using g but implicitly assuming that it represents $g_{\max}$. It is straightforward to show that the matrix elements of $\mathcal{M}^{s=2,g}_{\tau_4}$

are obtained by:

$$\langle\sigma_i|\mathcal{M}^{s,g}_{\tau_4}|\sigma_j\sigma_k\rangle = \sum_{\sigma_l}\big[\langle\sigma_i|\mathcal{M}^{s-1,g}_{\tau_1}|\sigma_j\sigma_\ell\rangle\langle\sigma_j|\mathcal{M}^{s-1,g}_{\tau_2}|\sigma_k\sigma_\ell\rangle \times \langle\sigma_k|\mathcal{M}^{s-1,g}_{\tau_3)}|\sigma_i\sigma_\ell\rangle\big]. \quad (5)$$

Equation (5) is completely general, and it must be applied to all $t(g_{\max})$ triangles of type $s = 1$. Thus, we end up with $t(g_{\max} - 1)$ TM's describing the Boltzmann weights of the spin configurations corresponding to the same number of $s = 2$ triangles, where the influence of the spin at the central node has been already accounted for.

Next, we observe that the same operation can be performed to sum over the influence of all spins placed at the vertices introduced in the generation $g = g_{\max} - 1$. In such case, new 2×4 TM's $\mathcal{M}^{s=3,g}_{\tau}$ can be defined, the elements of which are expressed in terms of three $\mathcal{M}^{s=2,g}_{\tau'}$ matrices according to Eq. (5). In fact, the procedure can be repeated over and over, i.e., if we evaluate all matrices $\mathcal{M}^{s,g}_{\tau}$ from $s = 2$ to $s = g_{\max}$, we take into account the contribution of all configurations due to the spins placed in the interior sites, and we end up with one single 2×4 TM matrix $\mathcal{M}^{s=g,g}_{\tau_2}$, which depends on the spins in the sites 1, 2, and 3. The sum of its elements corresponds to the complete partition function $Z_{g_{\max}}$ at a preestablished value of T.

Equation (5) can be explicitly written as four independent recurrence relations in terms of the distinct matrix elements indicated by Eq. (3) as:

$$\begin{aligned}
a^{s,g}_{\tau_4} &= a^{s-1,g}_{\tau_1}a^{s-1,g}_{\tau_2}a^{s-1,g}_{\tau_3} + b^{s-1,g}_{\tau_1}b^{s-1,g}_{\tau_2}b^{s-1,g}_{\tau_3}\\
b^{s,g}_{\tau_4} &= a^{s-1,g}_{\tau_1}c^{s-1,g}_{\tau_2}d^{s-1,g}_{\tau_3} + b^{s-1,g}_{\tau_1}d^{s-1,g}_{\tau_2}c^{s-1,g}_{\tau_3}\\
c^{s,g}_{\tau_4} &= c^{s-1,g}_{\tau_1}d^{s-1,g}_{\tau_2}a^{s-1,g}_{\tau_3} + d^{s-1,g}_{\tau_1}c^{s-1,g}_{\tau_2}b^{s-1,g}_{\tau_3}\\
d^{s,g}_{\tau_4} &= c^{s-1,g}_{\tau_1}b^{s-1,g}_{\tau_2}d^{s-1,g}_{\tau_3} + d^{s-1,g}_{\tau_1}a^{s-1,g}_{\tau_2}c^{s-1,g}_{\tau_3}. \quad (6)
\end{aligned}$$

Since the matrix elements are Boltzmann weights, the iteration of the above recurrence relations leads to numerical divergences after a small number of steps. Therefore, it is convenient to rewrite the maps in terms of the free energy per particle

$$f^{s,g}_{\tau} = -\frac{T}{N(s)}\ln\big[a^{s,g}_{\tau} + b^{s,g}_{\tau} + c^{s,g}_{\tau} + d^{s,g}_{\tau}\big]. \quad (7)$$

Once $J_0 > 0$, one can verify that $a^{s,g}_{\tau} \geqslant b^{s,g}_{\tau}, c^{s,g}_{\tau}, d^{s,g}_{\tau}$. Therefore, it is convenient to define $x^{s,g}_{\tau} = b^{s,g}_{\tau}/a^{s,g}_{\tau}$, $y^{s,g}_{\tau} = c^{s,g}_{\tau}/a^{s,g}_{\tau}$, $z^{s,g}_{\tau} = d^{s,g}_{\tau}/a^{s,g}_{\tau}$, so that Eq. (7) becomes

$$f^{s,g}_{\tau} = -\frac{T}{N(s)}\big\{\ln\big[a^{s,g}_{\tau}\big] + \ln\big[1 + x^{s,g}_{\tau} + y^{s,g}_{\tau} + z^{s,g}_{\tau}\big]\big\}. \quad (8)$$

For large values of g, the iteration of Eq. (6) indicates that $x^{s,g}_{\tau}, y^{s,g}_{\tau}$, and $z^{s,g}_{\tau}$ becomes negligible in a few steps. Thus, we may consider $f^{s,g}_{\tau} = -\frac{T}{N(s)}\ln a^{s,g}_{\tau}$, and replace the maps for the matrix elements in Eq. (6) by:

$$\begin{aligned}
f^{s,g}_{\tau_4} &= -\frac{N(s-1)}{N(s)}\big[f^{s-1,g}_{\tau_1} + f^{s-1,g}_{\tau_2} + f^{s-1,g}_{\tau_3}\big]\\
&\quad -\frac{T}{N(s)}\big[\ln\big(1 + x^{s-1,g}_{\tau_1}x^{s-1,g}_{\tau_2}x^{s-1,g}_{\tau_3}\big)\big]\\
x^{s,g}_{\tau_4} &= \big(y^{s-1,g}_{\tau_2}z^{s-1,g}_{\tau_3} + x^{s-1,g}_{\tau_1}z^{s-1,g}_{\tau_2}y^{s-1,g}_{\tau_3}\big)/q^{s,g}_{\tau_4}\\
y^{s,g}_{\tau_4} &= \big(y^{s-1,g}_{\tau_1}z^{s-1,g}_{\tau_2} + z^{s-1,g}_{\tau_1}y^{s-1,g}_{\tau_2}x^{s-1,g}_{\tau_3}\big)/q^{s,g}_{\tau_4}\\
z^{s,g}_{\tau_4} &= \big(y^{s-1,g}_{\tau_1}x^{s-1,g}_{\tau_2}z^{s-1,g}_{\tau_3} + z^{s-1,g}_{\tau_1}y^{s-1,g}_{\tau_3}\big)/q^{s,g}_{\tau_4}, \quad (9)
\end{aligned}$$

where $q^{s,g}_{\tau_4} = 1 + x^{s-1,g}_{\tau_1}x^{s-1,g}_{\tau_2}x^{s-1,g}_{\tau_3}$

From the free energy per particle obtained by the iteration of the above maps, we can evaluate the entropy and specific heat by proceeding with the numerical derivatives with respect to the temperature. However, we can also rewrite Eq. (6) in a different way that allows us to compute a quantity that plays the role of the correlation length ξ. Indeed, it is well known that, in a linear system, the correlation length can be expressed by

$$\xi = 1/\ln(\eta/\epsilon), \quad (10)$$

where η and ϵ are the largest and smallest eigenvalues of the TM describing the nearest-neighbor interaction.

Although the evaluation of $f(T)$ requires us to work with 2×4 $\mathcal{M}^{s,g}_{\tau}$ matrices, it is also possible to define, for each value of $g_{\max}$, 2×2 squares matrices $\widehat{\mathcal{M}}^{g,g}_{\tau=1}$ just by carrying the partial trace over the different configurations depending on the states of one of the spins in the original triangle. The eigenvalues of $\widehat{\mathcal{M}}^{g,g}_{\tau=1}$ can be easily evaluated but, as discussed in Ref. [16], one should be careful when extending the expression for ξ in Eq. (10) to models defined on complex networks. Because of this, we proceed with the analysis of the behavior of $1/\ln(\eta/\epsilon)$ while avoiding to make a direct identification to the correlation length. Thus, if we define

$$\widehat{\mathcal{M}}^{g,g}_{\tau=1} = \begin{bmatrix} p^{g,g}_1 & q^{g,g}_1 \\ q^{g,g}_1 & p^{g,g}_1 \end{bmatrix} = \begin{bmatrix} a^{g,g}_1 + b^{g,g}_1 & c^{g,g}_1 + d^{g,g}_1 \\ c^{g,g}_1 + d^{g,g}_1 & a^{g,g}_1 + b^{g,g}_1 \end{bmatrix}, \quad (11)$$

it is straightforward to obtain the eigenvalues $\eta^{g,g}_1 = p^{g,g}_1 + q^{g,g}_1$ and $\epsilon^{g,g}_1 = p^{g,g}_1 - q^{g,g}_1$.

IV. RESULTS

As discussed in the previous section, to obtain the results for a particular generation $g_{\max}$ one needs to know the radii and center of each circle in the AP. Therefore, in order to optimize the numerical procedure, we initially determine and store all data related to the geometry of the model. The exponential increase of the number of circles is reflected in the storage requirements, e.g., when increasing $g_{\max}$ from 15 to 16 the data file increases from ~ 2 GB to ~ 3.4 GB. This data size also impacts the required memory to address and carry on the computation of the partition function involving 2.1×10^7 individual triangles. Because of the quality of the results obtained for $g_{\max} = 15$, and of the much larger computational effort to go beyond this system size, we adopted $g_{\max} \leqslant 15$. In the following, we present the results for $g_{\max} = 5, 7, 10, 13$, and 15. The numerical calculations of the free energy $f(T)$ were made with 16 significant digit variables, as to obtain reliable values for the entropy $s(T)$ and the specific heat $c(T)$ through numerical derivatives of $f(T)$. The value of $1/\ln(\eta/\epsilon)$ is also evaluated with 16-digit precision.

In Fig. 2 we show the behavior of the free energy and entropy per spin as a function of the temperature, for $\alpha = 0.5$ and 0.8. It is important to remark that, once the value of J_{ij} is

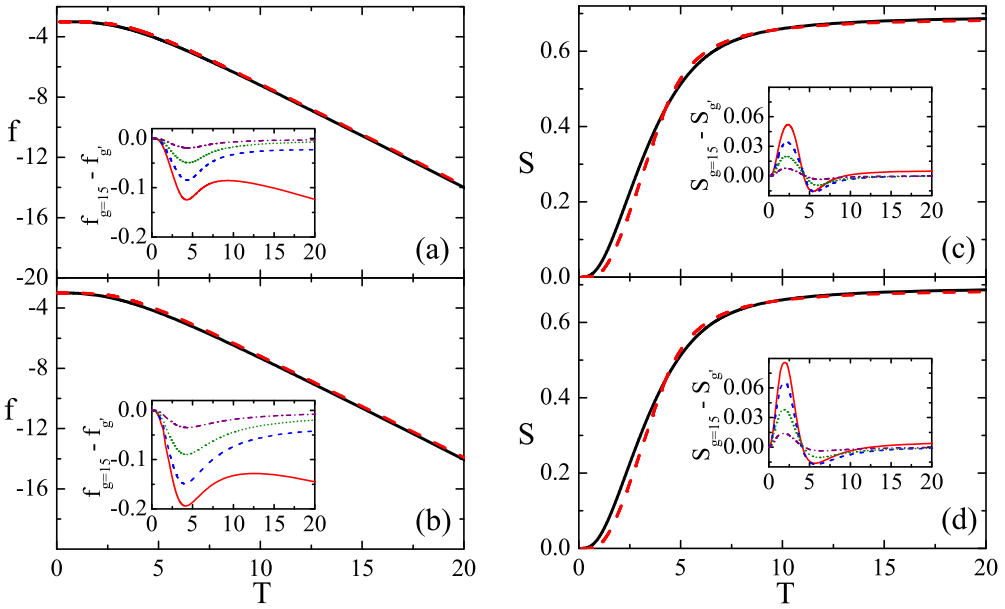

FIG. 2. Behavior of $f(T)$ [(a) and (b)] and $s(T)$ [(c) and (d)] for $g_{\max} = 5$ (red dashes) and 15 (black solid line), and $\alpha = 0.5$ [(a) and (c)] and 0.8 [(b) and (d)]. To enable a comparison of the curves for different values of $g_{\max}$, the values of J_0 were chosen in such a way that $f(T = 0) = -3$, as observed for the uniform model with $J_0 = 1$. As a consequence, the high temperature limit, when $s \to ln2$, is observed in the same range of values of T,$\forall g_{\max}$,α. The inset of all panels highlight the convergence of the results as $g_{\max}$ increases, by displaying the corresponding differences from $g' = 5$ (red solid line), 7 (blue dashes), 10 (green dots), and 13 (violet dot-dashes), to $g_{\max} = 15$.

not constant, the average energy per particle strongly depends on the model parameters. In the particular case expressed by Eq. (1), the average value of the coupling constants increase with g when $\alpha > 0$. Therefore, in order to better compare the results for different $g_{\max}$ values, it is wise to let J_0 change with $g_{\max}$. This is done by requiring that, for any $g_{\max}$, the free energy per spin at $T = 0$ assumes the same value, which is chosen to be -3 in order to reproduce the value of the uniform value ($\alpha = 0$). A similar procedure was introduced when analyzing the model where J_{ij} depends on the degree of the nodes i and j [16]. These features are well reflected by the shape of the curves. We observe that, independently of $g_{\max}$ and α, the limit of high temperatures, where $s(t) \sim \ln 2$ starts roughly at the same value of T.

Figure 3 shows the behavior of the specific heat as a function of the temperature for the same values of $g_{\max}$ and α. The curves are characterized by soft maxima $c_{\max}$, all of which occur in the same temperature range. They display no evidence of a divergence or any nonanalytic behavior that could hint for a magnetic phase transition. As observed in Sec. I, similar behavior has been verified for other magnetic models on the AN, or even for the uniform Ising model on other network types, such as the $\gamma \in [0,3]$ range of the scale-free Barabasi-Albert type [17]. The tendency of $c_{\max}$ is to decrease as $g_{\max}$ or α increases. Larger values of α cause stronger dependency of J_{ij} with respect to the distance between nodes, weakening the importance of the coupling between spins placed inside large circles, which are inserted in the network in the first generations and have large number of neighbors. A similar effect is introduced in the model investigated in Ref. [16], but a comparison of the corresponding specific heat curves indicate the oppositive tendency, i.e., $c_{\max}$ increases as α increases.

Although the specific heat curves do not present any sign of divergence, it is still possible to assess the existence of some critical behavior by the presence of a numerical divergence

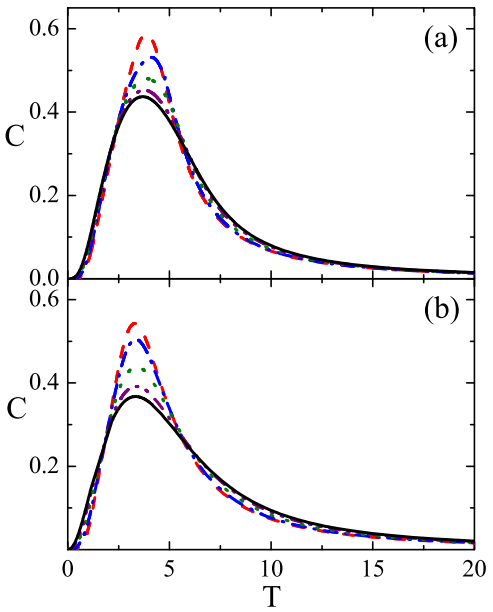

FIG. 3. Behavior of $c(T)$ for $g_{\max} = 5$ (red dashes), 7 (blue dot-dashes), 10 (green dots), 13 (violet dot-dot-dashes), and 15 (black solid line), and (a) $\alpha = 0.5$ and (b) 0.8. All curves follow the same Schottky profile. Because of the adequate definition of J_0, the smooth peaks always occur in the same temperature range. No indication of a singular behavior at a finite temperature has been detected. $g' = 5$ (red solid line), 7 (blue dashes), 10 (green dots), and 13 (violet dot-dashed line), to $g_{\max} = 15$.

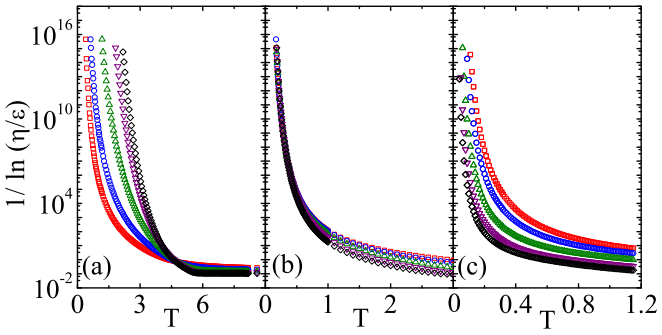

FIG. 4. Behavior of $1/\ln(\eta/\epsilon)$ as a function of temperature for $g_{\max} = 5$ (red squares), 7 (blue circles), 10 (green up-triangles), 13 (violet down-triangles) and 15 (black diamonds). (a), (b), and (c) illustrate the different behavior of the divergence temperature T_d for $\alpha = 0.5, 0.743$, and 0.87.

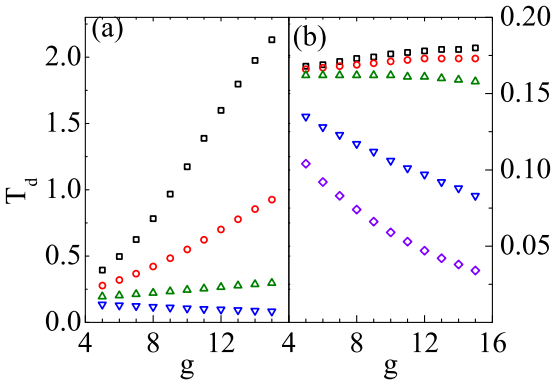

FIG. 5. Behavior of $T_d(g)$ as a function of $g_{\max}$ for different α. In (a), results for $\alpha = 0.5, 0.6, 0.7$, and 0.8, are identified by black squares, red circles, green up-triangles, and blue down-triangles, respectively. With exception of $\alpha = 0.8$, T_d increases with $g_{\max}$. In (b) $\alpha = 0.7, 0.743, 0.75, 0.8$, and 0.87 are identified by black squares, red circles, green up-triangles, blue down-triangles, and violet diamonds. While T_d increases when $\alpha = 0.7$ and approaches a constant plateau when $\alpha = 0.743$, it decreases with g when $\alpha > 0.743$.

(values greater than 10^{16}) for the quantity $1/\ln(\eta/\epsilon)$. In Fig. 4 we shows how this variable depends on the value of T for the same values of α and $g_{\max}$. It is observed that, on decreasing the value of T, a numerical divergence is observed at a well-defined value $T_d = T_d(g)$. For $\alpha = 0.5$ $T_d(g)$ increases with $g_{\max}$, while the opposite behavior is observed for $\alpha = 0.87$. In this situation, $T_d(g)$ vanishes exponentially when $g \to \infty$. The crossover between the two different regimes is observed, for $g_{\max} = 15$, to occur at $\alpha = \alpha_c \simeq 0.743$.

To put this result in perspective, let us remind that, for the uniform Ising model on the AN, $T_d(g)$ increases linearly with g, a result that is well reproduced when we set $\alpha = 0$ in the current work. For the model with degree-dependent coupling constant [16], the same results are observed as long as $\mu < 1.0$, while $T_d(g)$ decreases with g when the exponent $\mu > 1.0$.

This behavior is very similar to what is shown in Fig. 4. Indeed, within the limits of our numerical investigation ($g_{\max} \leqslant 15$), we were able to determine the value $\alpha_c = 0.743$ for the change in the behavior of T_d. This is illustrated in Fig. 5. At this threshold value, $T_d(g)$ remains roughly independent of the generation g.

Nevertheless, it appears from Fig. 4 that T_d bears no correlation with other behavior of the system. For instance it lies well below the value of $c_{\max}$, and no alteration is observed in the Schottky profile for the specific heat at this value of α.

We evaluated the spontaneous magnetization $m(T,h = 0)$ and zero-field susceptibility $\chi(T,h = 0)$ by numerically differentiating the field-dependent free energy. To this purpose, it is necessary to replace Eq. (9) by a larger set of maps, as explained in the Appendix. Figures 6 and 7 illustrate, respectively, the behavior of $m(T,h = 0)$ and $\chi(T,h = 0)$ for some typical values of α and five different $g_{\max} \in [5,15]$. We emphasize that, much as occurred with $1/\ln(\eta/\epsilon)$, the behavior of $m(T,h = 0)$ and $\chi(T,h = 0)$ depend on the chosen value of α and its relation to $\alpha_c \simeq 0.743$. For $\alpha < \alpha_c$, a plateau at $m \simeq 1$ appears in the region of small T, the width of which is nearly $g_{\max}$ independent. This almost horizontal structure is followed by a monotonic decrease of $m(T,h = 0)$ for larger T. If $\alpha = 0$, a pure exponential decay extends to the rest of the T axis, as reported previously for a homogeneous system where $J_{ij} = J_0, \forall i,j$ (see Fig. 2 of Ref. [15]). Finite-size effects appear in the form of deviations to a slower decrease regime, which sets in at larger and larger values of T as $g_{\max}$ increases. Such effect gives rise to $g_{\max}$-dependent peaks in the susceptibility $\chi(T,0)$.

For $0 < \alpha < 0.743$, the $g_{\max}$-independent plateau persists, although its width decreases as α increases. This is illustrated in the Fig. 6(a) for $\alpha = 0.5$, which also indicates that the exponential decay does not preserve the previously described $\alpha = 0$ pattern. As $g_{\max}$ increases, the corresponding $m_g(T,0)$ curves are marked by a much steeper decrease, which starts at values of T slightly smaller than those for the previous values of $g_{\max}$. Figure 6(a) also shows that the descent phase is marked by several changes in the slope of the curves, with the result that, given two values g and g', $m_g(T,0)$ and $m_{g'}(T,0)$ may cross each other several times. Nevertheless, for sufficiently large values of T, $m_g(T,0) < m_{g-1}(T,0)$, as also occurs when $\alpha = 0$.

These traits, which are typical for all values of α in the quoted interval, are also reflected in the behavior of

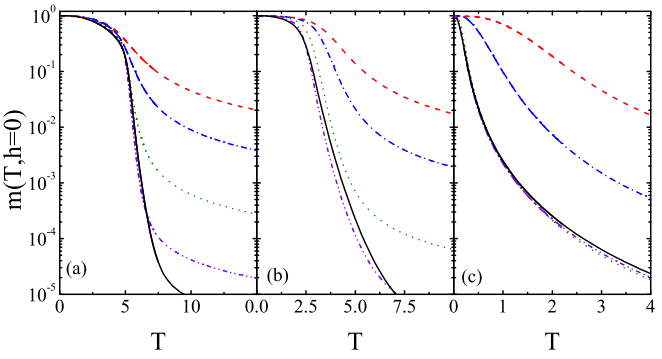

FIG. 6. Behavior of $m(T,h = 0)$ as a function of T for $g_{\max} = 5$ (red dashes), 7 (blue dot-dashes), 10 (green dots), 13 (violet dot-dot-dashes), and 15 (black solid line), (a), (b) and (c) correspond, respectively, to $\alpha = 0.5, 0.743$, and 1.3.

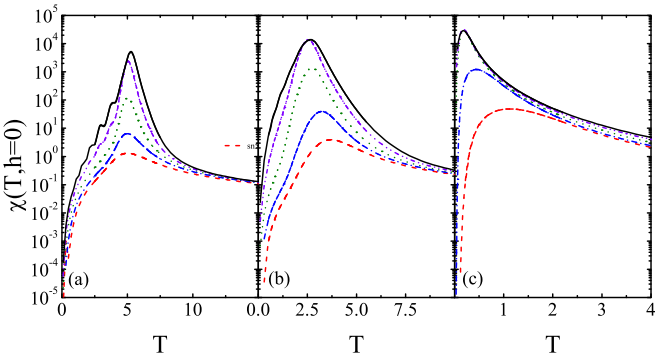

FIG. 7. Behavior of $\chi(T,h=0)$ as a function of T for $g_{\max}=5$ (red dashes), 7 (blue dot-dashes), 10 (green dots), 13 (violet dot-dot-dashes), and 15 (black solid line), Panels (a), (b) and (c) correspond, respectively, to $\alpha=0.5$, 0.743, and 1.3.

$\chi_g(T,h=0)$ as a function of T, which are shown in Fig. 7(a): a sharp (but otherwise smooth) peak develops at a value of T that can be identified with the largest slope of $\log[m(T,0)]$ as a function of T. We find that, for a fixed α, the maxima of $\chi_g(T,0)$ occur at larger values of T as $g_{\max}$ increases. Figure 7(a) also illustrates that the height of the peak increases with $g_{\max}$ but, much as observed when $\alpha=0$, there is no indication that a true singularity should be found in the $g\to\infty$ limit. Our results also show that, for a fixed $g_{\max}$, the height of these peaks increases with α.

A quite interesting feature in the behavior of $\chi_g(T,0)$ is the noticeable presence of a number of wiggles for the range of values of T smaller than the peak temperature. Their presence, which becomes evident for larger values of $g_{\max}$, occur at approximately equally spaced values of T. The difference between the logarithm of the heights of two successive wiggles remains also approximately constant. We could not identify their presence for values of T larger than the peak temperature.

When $\alpha>0.743$, the numerical results suggest that $m(T>0,0)=0$ in the $g\to\infty$ limit, much in the same way as the model investigated in Ref. [16]. Indeed, after a very small plateau at $m=1$, the width of which rapidly becomes negligible as $g_{\max}$ increases, $m_g(T,0)$ decays exponentially to zero. Once we are limited to rather small

values of $g_{\max}$, in Fig. 6(c) we show results for $\alpha=1.3$, where these features become quite evident. Figure 7(c) shows the evolution of $\chi_g(T,0)$ as a function of T for the same α and five values of $g_{\max}$. We notice that the peaks are still present, but they move towards smaller values of T as $g_{\max}$ increases. In fact, for all values of α, the change of the location of these peaks on the T axis follows the same tendency observed for the divergence of the $1/\ln(\eta/\epsilon)$ (see Fig. 4), although the actual values of T where the two events occur do not coincide. This is also verified when we consider $\alpha=\alpha_c$, as shown in Fig. 7(b). We notice that the $\chi_g(T,0)$ peaks remain at a rather fixed value of $T\neq T_d$. Finally, Fig. 6(b) illustrates the behavior of $m_g(T,0)$ at α_c, where a monotonic decrease in the width of the plateau can be observed.

V. DISCUSSION AND CONCLUSIONS

In this work we studied the Ising model on the AP. Here we consider ferromagnetic interactions that depend on the distance between the centers of the circles in the AP where the Ising spins are placed. In opposition to previous AN models, in which the interactions depend on the network topology, the explicit dependence of magnetic interactions on the geometric properties of the packing turns out to destroy the exact scale invariance of the system. This fact causes increased difficulties to perform the evaluation of the partition function within a TM framework, as compared to models where the packing geometry plays no role.

Despite this difficult, which restricted the work to a relatively small number of packing generation, we were able to characterize the most important features of the model. The characterization of three thermodynamic quantities, free energy, entropy, and specific heat, confirmed that their qualitative behavior is much like those in previous models.

The dependence of the quantity $1/\ln(\eta/\epsilon)$ as function of T indicates two disjoint ranges of values of α where, independently of the value of T, a well-defined magnetic ordering can, or cannot, be found.

This evidence, which is similar to the observed behavior of $1/\ln(\eta/\epsilon)$ in a distinct model [16], is confirmed by the evaluation of $m(T,0)$ and $\chi(T,0)$ for different values of α. We have found, however, that the magnetic behavior offers a more complex pattern as compared to that of the quoted model. We remind that the geometrical dependence of J_{ij} has a greater degree of inhomogeneity, once spins located on nodes with the same degree interact with their neighbors in different ways. This may be a reason for richer and more diverse patterns.

Finally, we mention the possibility of defining other ferromagnetic models on the AP where further geometrical properties of the packing are taken into account. One of them would consider that the magnetic moments in each circle center were to represent the global magnetic property of all spins placed inside the corresponding AP circle drawn on the top of a plane filled with equally spaced spins. In such case, a factor increasing with $r_i^2 r_j^2$ should be inserted in Eq. (1). We point out that this possibility should bring the model closer to a realistic model. However, one major difficult in this approach is that either the magnitude of the coupling or of the magnetic effective moment should be dependent on T.

ACKNOWLEDGMENTS

The authors acknowledge the financial support of Brazilian agencies Conselho Nacional de Desenvolvimento Científico e Tecnológico (CNPq), Coordenação de Aperfeiçoamento de Pessoal de Nível Superior (CAPES), and Fundação de Amparo à Pesquisa do Estado da Bahia (FAPESB). R.F.S.A. benefits from the support of the Instituto Nacional de Ciência e Tecnologia para Sistemas Complexos (INCT-SC). The authors thank Prof. H. J. Herrmann and Prof. J. S. Andrade Jr. for helpful discussions and suggestions.

APPENDIX

Here we provide the generalization of the Eqs. (3)–(9) in Sec. III, when the spins are subject to a magnetic field of magnitude h. We start with the elementary triangles in a field-free situation and, when we put together three triangles of type s to assemble a $s+1$ triangle, the effect of the field

is added only at the vertex that belongs simultaneously to all three s triangles. This assures that the magnitude of field acting on each spin is the same, with exception of the three outermost spins, which remain field free. However, their influence in the value of the magnetization is vanishingly small as g increases.

(i) Due to the up-down symmetry break induced by the field, new matrix elements are required for the field-dependent form of the matrix in Eq. (3):

$$\mathcal{M}_{\tau_1}^{s,g} = \begin{bmatrix} a_{\tau_1}^{s,g} & b_{\tau_1}^{s,g} & c_{\tau_1}^{s,g} & d_{\tau_1}^{s,g} \\ \bar{d}_{\tau_1}^{s,g} & \bar{c}_{\tau_1}^{s,g} & \bar{b}_{\tau_1}^{s,g} & \bar{a}_{\tau_1}^{s,g} \end{bmatrix}. \tag{A1}$$

(ii) Equation (4) does not become field dependent, as explained above.

(iii) Field-dependent form of Eq. (5):

$$\langle\sigma_i|\mathcal{M}_{\tau_4}^{s,g}|\sigma_j\sigma_k\rangle = \sum_{\sigma_l}\big[\langle\sigma_i|\mathcal{M}_{\tau_1}^{s-1,g}|\sigma_j\sigma_\ell\rangle\langle\sigma_j|\mathcal{M}_{\tau_2}^{s-1,g}|\sigma_k\sigma_\ell\rangle \times \langle\sigma_k|\mathcal{M}_{\tau_3)}^{s-1,g}|\sigma_i\sigma_\ell\rangle\big]\exp(\beta h\sigma_\ell). \tag{A2}$$

(iv) Field-dependent form of Eq. (6):

$$\begin{aligned}
a_{\tau_4}^{s,g} &= a_{\tau_1}^{s-1,g}a_{\tau_2}^{s-1,g}a_{\tau_3}^{s-1,g}r + b_{\tau_1}^{s-1,g}b_{\tau_2}^{s-1,g}b_{\tau_3}^{s-1,g}t \\
b_{\tau_4}^{s,g} &= a_{\tau_1}^{s-1,g}c_{\tau_2}^{s-1,g}\bar{d}_{\tau_3}^{s-1,g}r + b_{\tau_1}^{s-1,g}d_{\tau_2}^{s-1,g}\bar{c}_{\tau_3}^{s-1,g}t \\
c_{\tau_4}^{s,g} &= c_{\tau_1}^{s-1,g}\bar{d}_{\tau_2}^{s-1,g}a_{\tau_3}^{s-1,g}r + d_{\tau_1}^{s-1,g}\bar{c}_{\tau_2}^{s-1,g}b_{\tau_3}^{s-1,g}t \\
d_{\tau_4}^{s,g} &= c_{\tau_1}^{s-1,g}\bar{b}_{\tau_2}^{s-1,g}\bar{d}_{\tau_3}^{s-1,g}r + d_{\tau_1}^{s-1,g}\bar{a}_{\tau_2}^{s-1,g}\bar{c}_{\tau_3}^{s-1,g}t \\
\bar{d}_{\tau_4}^{s,g} &= \bar{c}_{\tau_1}^{s-1,g}b_{\tau_2}^{s-1,g}d_{\tau_3}^{s-1,g}t + \bar{d}_{\tau_1}^{s-1,g}a_{\tau_2}^{s-1,g}c_{\tau_3}^{s-1,g}r \\
\bar{c}_{\tau_4}^{s,g} &= \bar{c}_{\tau_1}^{s-1,g}d_{\tau_2}^{s-1,g}\bar{a}_{\tau_3}^{s-1,g}t + \bar{d}_{\tau_1}^{s-1,g}c_{\tau_2}^{s-1,g}\bar{b}_{\tau_3}^{s-1,g}r \\
\bar{b}_{\tau_4}^{s,g} &= \bar{a}_{\tau_1}^{s-1,g}\bar{c}_{\tau_2}^{s-1,g}d_{\tau_3}^{s-1,g}t + \bar{b}_{\tau_1}^{s-1,g}\bar{d}_{\tau_2}^{s-1,g}c_{\tau_3}^{s-1,g}r \\
\bar{a}_{\tau_4}^{s,g} &= \bar{a}_{\tau_1}^{s-1,g}\bar{a}_{\tau_2}^{s-1,g}\bar{a}_{\tau_3}^{s-1,g}t + \bar{b}_{\tau_1}^{s-1,g}\bar{b}_{\tau_2}^{s-1,g}\bar{b}_{\tau_3}^{s-1,g}r
\end{aligned} \tag{A3}$$

where $r = \exp(\beta h) = t^{-1}$.

(v) The two free-energy definitions given by Eqs. (7) and (8) are not changed by the presence of the field.

(vi) To account for the new matrix elements, new normalized coefficients are introduced, in a similar way as done in the paragraph between Eqs. (7) and (8): $\bar{x}_\tau^{s,g} = \bar{b}_\tau^{s,g}/a_\tau^{s,g}$, $\bar{y}_\tau^{s,g} = \bar{c}_\tau^{s,g}/a_\tau^{s,g}$, $\bar{z}_\tau^{s,g} = \bar{d}_\tau^{s,g}/a_\tau^{s,g}$, $\bar{w}_\tau^{s,g} = \bar{a}_\tau^{s,g}/a_\tau^{s,g}$.

(vii) Field-dependent form of Eqs. (9):

$$\begin{aligned}
f_{\tau_4}^{s,g} &= -\frac{N(s-1)}{N(s)}\big[f_{\tau_1}^{s-1,g} + f_{\tau_2}^{s-1,g} + f_{\tau_3}^{s-1,g}\big] \\
&\quad - \frac{T}{N(s)}\big[\ln\big(r + x_{\tau_1}^{s-1,g}x_{\tau_2}^{s-1,g}x_{\tau_3}^{s-1,g}t\big)\big] \\
x_{\tau_4}^{s,g} &= \big(y_{\tau_2}^{s-1,g}\bar{z}_{\tau_3}^{s-1,g}r + x_{\tau_1}^{s-1,g}z_{\tau_2}^{s-1,g}\bar{y}_{\tau_3}^{s-1,g}t\big)/q_{\tau_4}^{s,g} \\
y_{\tau_4}^{s,g} &= \big(y_{\tau_1}^{s-1,g}\bar{z}_{\tau_2}^{s-1,g}r + z_{\tau_1}^{s-1,g}\bar{y}_{\tau_2}^{s-1,g}x_{\tau_3}^{s-1,g}t\big)/q_{\tau_4}^{s,g} \\
z_{\tau_4}^{s,g} &= \big(y_{\tau_1}^{s-1,g}\bar{x}_{\tau_2}^{s-1,g}\bar{z}_{\tau_3}^{s-1,g}r + z_{\tau_1}^{s-1,g}\bar{w}_{\tau_2}^{s-1,g}\bar{y}_{\tau_3}^{s-1,g}t\big)/q_{\tau_4}^{s,g} \\
\bar{z}_{\tau_4}^{s,g} &= \big(\bar{y}_{\tau_1}^{s-1,g}x_{\tau_2}^{s-1,g}z_{\tau_3}^{s-1,g}t + \bar{z}_{\tau_1}^{s-1,g}y_{\tau_3}^{s-1,g}r\big)/q_{\tau_4}^{s,g} \\
\bar{y}_{\tau_4}^{s,g} &= \big(\bar{y}_{\tau_1}^{s-1,g}z_{\tau_2}^{s-1,g}\bar{w}_{\tau_3}^{s-1,g}t + \bar{z}_{\tau_1}^{s-1,g}y_{\tau_2}^{s-1,g}\bar{x}_{\tau_3}^{s-1,g}r\big)/q_{\tau_4}^{s,g} \\
\bar{x}_{\tau_4}^{s,g} &= \big(\bar{w}_{\tau_1}^{s-1,g}\bar{y}_{\tau_2}^{s-1,g}z_{\tau_3}^{s-1,g}t + \bar{x}_{\tau_1}^{s-1,g}\bar{z}_{\tau_2}^{s-1,g}y_{\tau_3}^{s-1,g}r\big)/q_{\tau_4}^{s,g} \\
\bar{w}_{\tau_4}^{s,g} &= \big(\bar{w}_{\tau_1}^{s-1,g}\bar{w}_{\tau_2}^{s-1,g}\bar{w}_{\tau_3}^{s-1,g}t + \bar{x}_{\tau_1}^{s-1,g}\bar{x}_{\tau_2}^{s-1,g}\bar{x}_{\tau_3}^{s-1,g}r\big)/q_{\tau_4}^{s,g}
\end{aligned} \tag{A4}$$

where $q_{\tau_4}^{s,g} = r + x_{\tau_1}^{s-1,g}x_{\tau_2}^{s-1,g}x_{\tau_3}^{s-1,g}t$.

[1] R. Albert and A.-L. Barabási, Rev. Mod. Phys. **74**, 47 (2002).
[2] M. Newman, SIAM Rev. **45**, 167 (2003).
[3] S. Boccaletti, V. Latora, Y. Moreno, M. Chavez, and D.-U. Hwang, Phys. Rep. **424**, 175 (2006).
[4] L. da F. Costa, F. A. Rodrigues, G. Travieso, and P. R. V. Boas, Adv. Phys. **56**, 167 (2007).
[5] P. Erdös and A. Rényi, Publ. Math., Debrecen **6**, 290 (1959).
[6] D. J. Watts and S. H. Strogatz, Nature (London) **393**, 440 (1998).
[7] A.-L. Barabási and R. Albert, Science **286**, 509 (1999).
[8] E. Ravasz and A.-L. Barabási, Phys. Rev. E **67**, 026112 (2003).
[9] J. S. Andrade, H. J. Herrmann, R. F. S. Andrade, and L. R. da Silva, Phys. Rev. Lett. **94**, 018702 (2005).
[10] J. P. K. Doye and C. P. Massen, Phys. Rev. E **71**, 016128 (2005).
[11] A. Aleksiejuk, J. A. Hoyst, and D. Stauffer, Physica A (Amsterdam) **310**, 260 (2002).
[12] S. N. Dorogovtsev, A. V. Goltsev, and J. F. F. Mendes, Phys. Rev. E **66**, 016104 (2002).
[13] A. V. Goltsev, S. N. Dorogovtsev, and J. F. F. Mendes, Phys. Rev. E **67**, 026123 (2003).
[14] S. N. Dorogovtsev, A. V. Goltsev, and J. F. F. Mendes, Rev. Mod. Phys. **80**, 1275 (2008).
[15] R. F. S. Andrade and H. J. Herrmann, Phys. Rev. E **71**, 056131 (2005).
[16] R. F. S. Andrade, J. S. Andrade, and H. J. Herrmann, Phys. Rev. E **79**, 036105 (2009).
[17] C. V. Giuraniuc, J. P. L. Hatchett, J. O. Indekeu, M. Leone, I. Pérez Castillo, B. Van Schaeybroeck, and C. Vanderzande, Phys. Rev. Lett. **95**, 098701 (2005).
[18] C. V. Giuraniuc, J. P. L. Hatchett, J. O. Indekeu, M. Leone, I. Pérez Castillo, B. Van Schaeybroeck, and C. Vanderzande, Phys. Rev. E **74**, 036108 (2006).
[19] N. A. M. Araújo, R. F. S. Andrade, and H. J. Herrmann, Phys. Rev. E **82**, 046109 (2010).
[20] V. S. T. Silva, R. F. S. Andrade, and S. R. Salinas, Phys. Rev. E **90**, 052112 (2014).
[21] J. C. Lagarias, C. L. Mallows, and A. R. Wilks, Am. Math. Mon. **109**, 338 (2002).
[22] H. J. Herrmann, G. Mantica, and D. Bessis, Phys. Rev. Lett. **65**, 3223 (1990).
[23] C. N. Kaplan, M. Hinczewski, and A. N. Berker, Phys. Rev. E **79**, 061120 (2009).
[24] A. L.Cardoso and R. F. S. Andrade and A. M. C. Souza, Phys. Rev. B **78**, 214202 (2008).
[25] I. N. de Oliveira, F. A. B. F. de Moura, M. L. Lyra, J. S. Andrade, and E. L. Albuquerque, Phys. Rev. E **81**, 030104 (2010).
[26] X.-P. Xu, W. Li, and F. Liu, Phys. Rev. E **78**, 052103 (2008).
[27] A. M. C. Souza and R. F. S. Andrade, J. Phys. A **46**, 145102 (2013).

[28] I. N. de Oliveira, F. A. B. F. de Moura, M. L. Lyra, J. S. Andrade, and E. L. Albuquerque, Phys. Rev. E **79**, 016104 (2009).
[29] F. W. S. Lima, André A. Moreira, and Ascânio D. Araújo, Phys. Rev. E **86**, 056109 (2012).
[30] L. da Silva, R. C. Filho, D. Soares, A. Macedo-Filho, U. Fulco, and E. Albuquerque, Physica A (Amsterdam) **392**, 1532 (2013).
[31] L. F. da Silva, R. N. Costa Filho, A. R. Cunha, A. Macedo-Filho, M. Serva, U. L. Fulco, and E. L. Albuquerque, J. Stat. Mech.: Theor. Expt. (2013) P05003.
[32] M. Serva, U. L. Fulco, and E. L. Albuquerque, Phys. Rev. E **88**, 042823 (2013).
[33] M. Serva, U. L. Fulco, and E. L. Albuquerque, J. Stat. Mech.: Theor. Expt. (2014) P01010.